THE JOURNAL OF PHYSICAL CHEMISTRY B

Article

pubs.acs.org/JPCB

Quantification of the Influence of Endotoxins on the Mechanics of Adult and Neonatal Red Blood Cells

Hiroaki Ito,[†,‡] Navina Kuss,[§] Bastian E. Rapp,[∥] Masatoshi Ichikawa,[†] Thomas Gutsmann,[⊥] Klaus Brandenburg,[⊥] Johannes M. B. Pöschl,[§] and Motomu Tanaka*[,‡,¶]

[†]Department of Physics, Graduate School of Science, Kyoto University, 606-8502 Kyoto, Japan

[‡]Institute of Physical Chemistry, University of Heidelberg, D69120 Heidelberg, Germany

[§]Department of Pediatrics, Clinic of Neonatology, University of Heidelberg, D69120 Heidelberg, Germany

[∥]Institute of Microstructure Technology (IMT), Karlsruhe Institute of Technology (KIT), 76344 Eggenstein-Leopoldshafen, Germany

[⊥]Research Center Borstel, D23845 Borstel, Germany

[¶]Institute for Integrated Cell-Material Science (WPI iCeMS), Kyoto University, 606-8501 Kyoto, Japan

Supporting Information

ABSTRACT: In this study, we physically modeled the influence of endotoxin-induced sepsis symptoms on human red blood cells (RBCs) by quantifying the impact of endotoxins on the cell mechanics by the analysis of Fourier-transformed mean square amplitude of shape fluctuation, called flicker spectroscopy. With the aid of a microfluidic diffusion chamber, we noninvasively determined principal mechanical parameters of human RBCs in the absence and presence of endotoxins for individual RBCs for the first time. Because of the elongation of saccharide chain length of endotoxins, we found an increase in the morphological transition from discocytes to echinocytes, and monotonic changes in the mechanical parameters. Since septic shocks often cause lethal risks of neonates, we measured the mechanical parameters of neonatal RBCs, and compared them to those of adult RBCs. The quantitative comparison reveals that neonatal RBCs are more susceptible to the effect of endotoxins than adult RBCs. Furthermore, coincubation with the antiseptic peptide P19-2.5 (Aspidasept) with endotoxin results in a slight suppression of the impact of the endotoxin. The strategy proposed in our study can potentially be applied for the quantitative diagnosis of RBCs based on mechanical readouts.

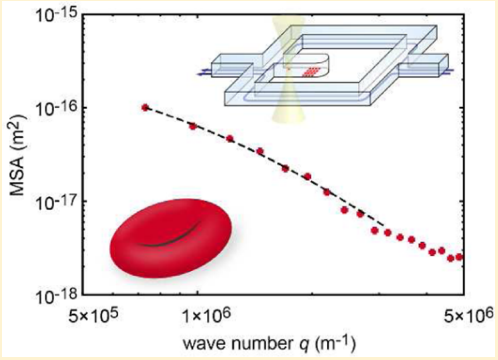

1. INTRODUCTION

Lipopolysaccharides (LPSs) are the major constituent of outer membranes of Gram-negative bacteria that guarantee the structural integrity of bacteria. LPSs are also known as endotoxins because of their capability to cause systematic inflammatory response syndromes in our body, such as sepsis.[1] The most fundamental building block of endotoxin is composed of six hydrocarbon chains and a hydrophilic group, called lipid A, which is further modified with additional inner and outer core saccharides. The complex LPSs with only inner core, which is the simplest form for the growth of Gram-negative bacteria, and both inner and outer cores are called LPS Re and LPS Ra, respectively.[2] To date, many studies have indicated that the septic shocks caused by the exposure to endotoxin have a significant consequence on the mechanics of red blood cells (RBCs). For example, Pöschl and Linderkamp measured the deformability (physically equivalent to the aspect ratio between the major axis and minor axis) of elliptically deformed RBCs from adults[3,4] and neonates,[5] i.e., newborn infants, under shear stresses, demonstrating that endotoxin causes more significant changes in the deformability of neonatal RBCs than adult RBCs. The exposure to group B *Streptococcus* leads to a significant decrease in the deformability under shear, i.e., RBCs became stiffer against the elongation and thus lose their capability for microcirculatory blood flow. This tendency was much more pronounced for neonatal RBCs than adult RBCs, as sepsis tends to be more critical for neonates whose prematured immune systems cannot fight against external intruders.[6] From the physical viewpoint, the change in the aspect ratio of RBC under mechanical stresses could be attributed to the shear deformation of a viscoelastic body, which have been investigated using optical tweezers[7,8] and optical stretchers[9−11] more recently. However, despite of major developments in impairing the progression of diseases and revealing cell mechanics, these approaches did not shed light on the impact of endotoxins on key mechanical parameters, such as the bending stiffness and surface tension.[12,13] Therefore, to clarify this general elasticity under the endotoxic conditions can

Received: February 14, 2015
Revised: May 25, 2015
Published: May 29, 2015

DOI: 10.1021/acs.jpcb.5b01544
J. Phys. Chem. B 2015, 119, 7837−7845

lead to deeper understanding and quantification of the diseased state and mechanical response of the RBCs.

Another experimental approach to determine the mechanical properties of membranes from the fluctuation of membrane shapes, called flicker spectroscopy, was developed after the pioneering study by Brochard and Lennon.[14] Here, the "flickering" of the local cell thickness observed by the phase contrast imaging was attributed to the thermal or nonthermal agitation against the bending energy of cell membranes described by Helfrich.[15] Brochard and Lennon assumed in their model that shear elastic energy of the cytoskeletal network could be neglected compared to the bending energy of the cell membrane due to the assumption of a planar membrane. To obtain information on the cell shape more directly, the following studies included shear elasticity to the theory, which is more appropriate to analyze the curved cell rims.[16,17] More recently, the confinement of membrane deviation due to the underlying cytoskeletal structure, i.e., spectrin network, was incorporated to the theory[13,18] to explain the gap between obtained shear moduli in the above models with experimental values obtained by static deformation experiments such as micropipet aspiration[19,20] and electro-deformation.[21,22] As it was pointed out by Yoon et al., this energetic term of the cytoskeletal confinement and the shear energy term of a single, polymerized cytoskeletal network lead to a similar formulation for the mean square amplitude of the contour fluctuation.[23,24] Within the framework, the spring constant γ of the harmonic potential that confines membranes adjacent to cytoskeletons can be replaced by the ratio between the shear elasticity μ and the membrane area A, μ/A. Recently, this model was refined to optimize to the analysis of the cross-sectional images of equatorial cell rims, which are usually obtained by phase contrast microscopy.[25] This model can quantify the spring constant of the cytoskeletal confinement, bending stiffness, and surface tension by the fitting of experimentally obtained mean square amplitude of shape fluctuation of RBCs. However, despite of the development in the theoretical analysis, the use of flicker spectroscopy to determine the impact of external stimuli, leading to septic shocks, on the membrane mechanics has been limited because of the difficulties in tracking changes in the mechanics of individual cells over time: A simple ensemble is not sufficient to capture the essential behavior of individual cells, which often express considerably inhomogeneous cell mechanics because of the aging of RBCs during their life-span of 120 days.

In the present paper, we apply the flicker spectroscopy and microfluidic systems to quantify the mechanics of individual cells under healthy and septic conditions. Here, we adopted a "diffusion chamber"[26] to analyze exactly the same individual cells. Since the use of diffusion chambers enables one to exchange the surrounding environment of cells within a few minutes, we tried to quantify not only impacts of endotoxins but also the curative effects of antiseptic peptide P19 (P19-2.5, Aspidasent) against them.[27]

2. EXPERIMENTAL SECTION

2.1. Sample Preparation. Adult and neonatal blood was drawn from healthy donors with the approval of the Ethical Committee of University of Heidelberg and the informed consent of donors and parents. PBS buffers (pH 7.4) with 130 mM NaCl, 10 mM glucose and 1 mg/mL Bovine serum albumin (BSA, Sigma-Aldrich, St. Louis, MO) was used as the buffer solution throughout the study, where 10 mM glucose is needed to keep the ATP level and the cytoskeletal remodeling during the measurements.[28,29] RBCs were extracted from the blood sample by 1/40 dilution, centrifugation and replacement of supernatant by the buffer: First, we diluted the sample blood by the buffer (blood:buffer = 4 μL:196 μL). Next, the obtained 200 μL solution was centrifuged (1000 rpm, 6 min) and the supernatant, which is 90% of the entire solution, was replaced by the PBS buffer. Then, we repeated the above process two times more. All human RBCs extracted in this process had the shape of a biconcave discoid (discocyte), as those under physiological condition are. Endotoxins, LPS Re and LPS Ra, were purified from bacterial strains *R*60 and *R*595 of *Salmenella enterica* serovar Minnesota,[30,31] while lipid A was obtained by hydrolysis of LPS Re.[32] The powders of lipid A, LPS Re and LPS Ra were dissolved in the PBS buffer at concentrations of 100 μg/mL, respectively. Antiseptic peptide P19-2.5 (P19, MW = 2711)[27,33,34] was premixed with a portion of 100 μg/mL LPS Ra solution at a concentration of 1 mg/mL. Using these endotoxin and endotoxin with antiseptic peptide solutions, we performed the following perfusion in the microfluidic diffusion chamber.

2.2. Microfluidic Diffusion Chamber. Figure 1a shows a schematic illustration of a microfluidic diffusion chamber. The flow channels were molded in a poly(dimethylsiloxane) (PDMS) resin, and enclosed by a glass coverslip. The mold for replicating the PDMS chips was manufactured via photolithography in SU-8 (type 2075, purchased from micro resist technology, Germany) using a maskless projection lithography system as described previously.[35] Briefly, SU-8 was spin-coated (30 s at 500 rpm, 55 s rest, 20 s at 3000 rpm) on cyclic olefin copolymer (COC, type TOPAS 6013S-04), prebaked (1 h at 75 °C, 4 h at 95 °C), exposed and postbaked

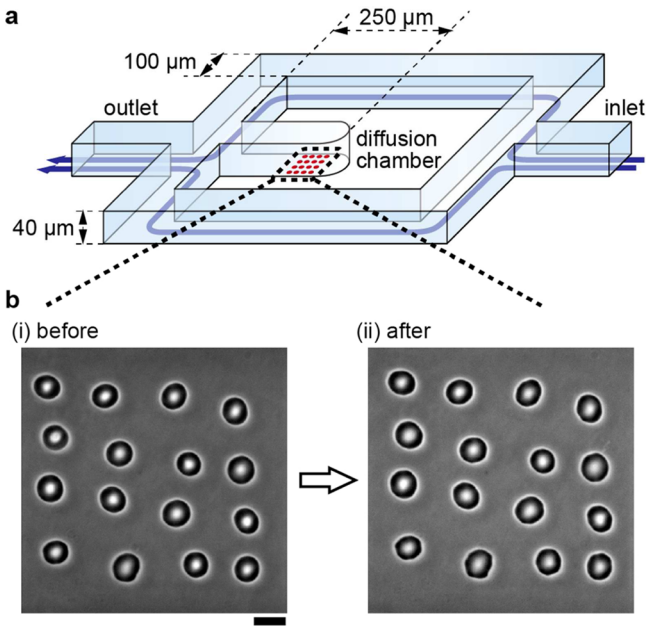

Figure 1. (a) Schematic of a microfluidic diffusion chamber. Blue arrows show the flow direction inside the channel. Substances dissolved in water can diffuse into the "diffusion chamber" in a controlled manner (see Supporting Information). (b) Full view of aligned red blood cells in the diffusion chamber before and after perfusion of LPS Ra 100 μg/mL solution inside the channel. Scale bar: 10 μm.

DOI: 10.1021/acs.jpcb.5b01544
J. Phys. Chem. B 2015, 119, 7837−7845

(2 min at 65 °C, 10 min at 95 °C) and developed in ethyl-L-lactate (purchased from Sigma-Aldrich, Germany) in an ultrasonic bath (5 min). After unset PDMS was poured on the mold, the air contained in the PDMS was degassed under vacuum for 1 h. Then, the PDMS was baked at 80 °C overnight. The microstructure was cut out of the mold, and the holes for inlet and outlet of solution were made. Finally, the glass coverslip and the PDMS chip were bonded by the surface treatment with a corona discharger (BD-20AC Laboratory Corona Treater, Electro-Technic Products) for 10 s each. The inlet and outlet holes were connected to silicon tubes via polytetrafluoroethylene (PTFE) tubes, and the inlet silicon tube was connected to a syringe. Then 16 RBCs were placed and aligned in the diffusion chamber (see Figure 1b) using an optical tweezers in approximately 20 min. Figure 1b shows RBCs before (i) and after (ii) perfusion of another kind of solution. This microfluidic device allows us to exchange the surrounding solute condition inside the diffusion chamber within a few minutes only by diffusion, i.e., without flow, at a desired timing and at a desired solute concentration (see Supporting Information for detail).

2.3. Microscopic Observation. The microfluidic device with aligned RBCs inside the chamber was set inside a thermostat (37 °C) on the stage of an optical microscope (TE-2000U, Nikon and Axiovert 200, Zeiss) with a ring aperture. After thermal equilibrium with constant temperature, we recorded 600 frames of temporal cell shapes with a ×100, N.A. = 1.3, oil-immersion objective lens and EM-CCD camera (C9743−13, Hamamatsu), resulting pixel size was 0.16 μm, or ×100, N.A. = 1.4 oil-immersion objective lens and CCD camera (C4742−95−12ER, Hamamatsu), pixel size 0.1 μm, for each cell. To obtain temporal ensemble average of shapes for each cell, exposure time and time interval of adjacent two frames were taken as 30.5 ms. Then, the inlet silicon tube filled with the buffer was replaced by the tube filled with endotoxin solution, and repeated the above record procedure. In the case of treatments of P19, the inlet silicon tube for LPS Ra solution was further replaced by the tube filled with LPS Ra and P19 solution, and the procedure was repeated. Note that the diffusion of solutes into the chamber is much faster than the thermal equilibration of the whole system with newly perfused solution (see Supporting Information).

2.4. Flicker Spectroscopy. The inset of Figure 2a shows a typical phase contrast image. Cell rim can be detected as the intensity peak of an intensity-gradient magnitude image obtained in ImageJ.[36] Whole rim detection of the captured cell images was performed by a custom routine in Igor Pro (WaveMetrics, Oregon). Briefly, in polar coordinate (r, φ), 360 discrete radial distance $r(\varphi)$ $(0 \le \varphi < 2\pi)$ for 360 deg from the center of mass to the rim were detected for each frame (Figure 2a). The fluctuation profiles, which are defined as the deviation from the time-averaged cell shapes, were Fourier-transformed into the mean square amplitudes as a function of wavenumber q:

$$\langle u(q)^2 \rangle = \left\langle \left| \frac{2}{N} \sum_{n=0}^{N-1} \{r(n\Delta x) - \langle r(n\Delta x) \rangle\} e^{2\pi i q n/N} \right|^2 \right\rangle \quad (1)$$

where $\langle\ \rangle$ denotes time average over the whole frames, $N = 360$ is the sampling number, and $\Delta x = 2\pi\langle r \rangle/N$. On the other hand, theoretically predicted mean square amplitude is described as

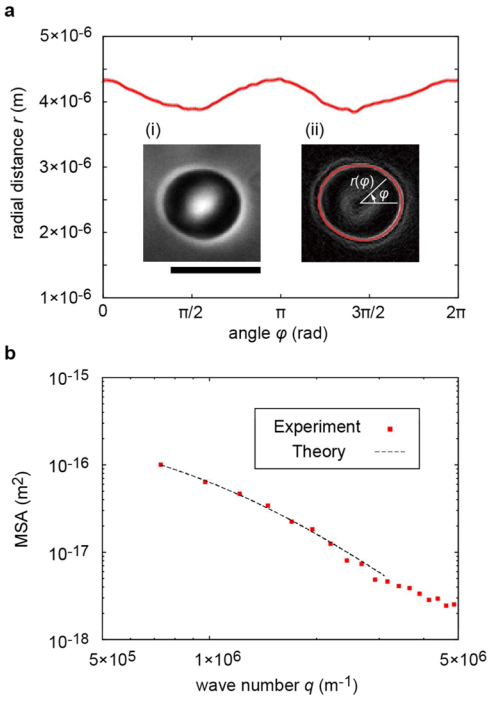

Figure 2. (a) Detected radial distance from the center of mass plotted versus angle φ $(0 \le \varphi < 2\pi)$. Typical examples of (i) the phase contrast image of a fluctuating red blood cell and (ii) the identified cell rim from the intensity gradient are presented as the insets. Scale bar: 10 μm. (b) Mean square amplitude of the shape fluctuation of the cell rim (red markers) and the best-fit result with theoretical model (dashed line). The fitting was performed from the third wavenumber mode to the maximum spatial resolution (see main text for details).

$$\langle u(q_x, y = 0)^2 \rangle = \frac{k_B T}{L} \sqrt{\frac{\kappa}{2(\sigma^2 - 4\kappa\gamma)}} \left(\frac{1}{\sqrt{2\kappa q_x^2 + \sigma - \sqrt{\sigma^2 - 4\kappa\gamma}}} - \frac{1}{\sqrt{2\kappa q_x^2 + \sigma + \sqrt{\sigma^2 - 4\kappa\gamma}}} \right) \quad (2)$$

where q_x is the continuous wavenumber corresponding to the experimental q, and L denotes one-dimensional length of a RBC.[24] Because eq 2 corresponds to the mean square amplitude of the cross-sectional line between a fluctuating planar membrane and a focal plane, it would be invalid for a closed and curved membrane of a RBC in a small wavenumber region. Thus, we performed the fitting with eq 2 over the third wavenumber mode ($\langle r \rangle q \ge 3$), where the gap between the mean square amplitudes of planar and spherical membrane becomes within 15%. Figure 2b exemplifies that eq 2 is sufficiently good to fit the experimental mean square amplitude in this wavenumber region. As previously demonstrated, the low wavenumber region is dominated by spring constant γ and surface tension σ, while the high wavenumber region is by bending stiffness κ.[24,37] The overall curve is determined as a combination of these mechanical parameters (see Figure S2 and Figure S3 in the Supporting Information).[37] From the best-fit result, we quantified the essential elastic coefficients for each

DOI: 10.1021/acs.jpcb.5b01544
J. Phys. Chem. B 2015, 119, 7837−7845

RBC: spring constant γ, bending stiffness κ and surface tension σ.[37] Coefficients of determination for the fittings were sufficiently high (above 0.999, see Table S1 in the Supporting Information for detail) with these three mechanical parameters. Note that spring constant of the cytoskeletal confinement γ is proportional to the shear modulus of membrane-cytoskeleton complex for a closed spherical membrane.

3. RESULTS

In the first step, we focused on the change in global cell shapes before and after the perfusion of endotoxins (Figure 3a). As exemplified in the figure, an adult RBC changed its shape after the perfusion of 100 μg/mL LPS Ra and 1 mg/mL P19 from (i) normal discocyte shape to (ii) faceted shape and (iii) echinocyte shape under the exposure to endotoxin. Figure 3b shows the fraction of the faceted cells and echinocytes in adult and neonatal RBCs in the presence of 100 μg/mL lipid A, LPS Re and LPS Ra after 15 min incubations. As presented in Figure 3b, both adult and neonatal discocytes were more transformed to echinocytes when the saccharide head groups of endotoxins became longer, but neonatal RBCs were much more susceptible to endotoxins (Figure 3b, red): The fractions of neonatal RBCs that underwent echinocytosis by the exposure to each endotoxin were more than the double of the corresponding values for adult RBCs. In fact, more than one-half of neonatal RBCs underwent echinocytosis in contact with LPS Re and LPS Ra. It should be noted that the osmolarity difference of these solutions was not significant: 304.8 ± 10.9, 298.5 ± 13.0, and 301.2 ± 12.1 mmol/kg for 100 μg/mL lipid A, 100 μg/mL LPS Re, and 100 μg/mL LPS Ra, respectively (mean ± SD, n = 10).

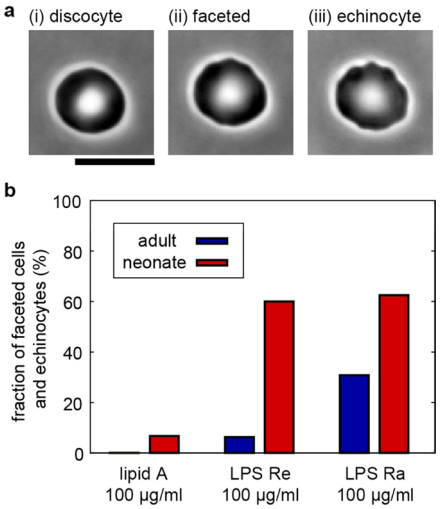

Figure 3. (a) Shape variations of a red blood cell after the treatment with endotoxins, ranging from (i) normal discocyte shape to (ii) faceted shape and (iii) echinocyte shape. Note that faceted cells and echinocytes are discriminated from discocytes once the spherical harmonics approximation fails, while there is no clear definition between faceted cells and echinocytes. Scale bar: 10 μm. (b) Fractions of the faceted cells and echinocytes in adult (blue) and neonatal (red) red blood cells after the incubation with 100 μg/mL lipid A, LPS Re, and LPS Ra for t = 15 min, indicating that neonatal red blood cells are much more susceptible to endotoxins.

To elucidate the impacts of endotoxins quantitatively beyond the phenomenological observation of ensembles, we measured the elastic constants of individual RBCs before and after the exposure to endotoxins by flicker spectroscopy. In this study only discocyte-like shape were subjected to the analysis, not only because the rim detection of echinocytes with drastic spicules is difficult but also because the large shape deviation from a smooth shape is no longer suitable for the comparison with the theoretical mean squared amplitude (eq 2). Thus, the evaluated values provide with the lower limit of the overall effect of endotoxins on RBCs. To quantify the tendency of scattered mechanical responses of individual cells, which is essential for living matters, we evaluated the relative changes in the mean values of the elastic constants together with their correlation coefficient in the ensembles (see Supporting Information). Figure 4 shows the individual (gray lines) and the mean (black thick lines) values of spring constant γ, which relates to shear elastic property of the cells, and bending stiffness κ of adult RBCs in the absence and presence of

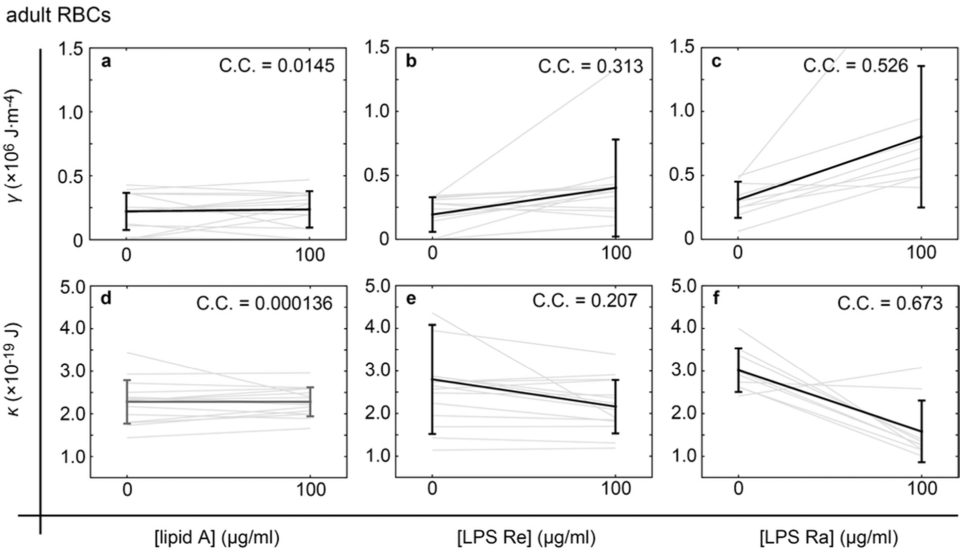

Figure 4. Impacts of endotoxins on the elastic properties of adult red blood cells. Individual (gray lines) and the mean (black thick lines) values of the spring constant γ in the absence and presence of 100 μg/mL (a) lipid A, (b) LPS Re, and (c) LPS Ra. The errors coincide with the standard deviations. (d–f) Changes in the bending stiffness κ caused by 100 μg/mL lipid A, LPS Re and LPS Ra, respectively.

DOI: 10.1021/acs.jpcb.5b01544
J. Phys. Chem. B 2015, 119, 7837–7845

endotoxins, i.e., 100 μg/mL portions of lipid A, LPS Re, and LPS Ra, respectively. First, lipid A had no impact on the mechanics of adult RBCs, which seems consistent with our ensemble observation that we found almost no sign of echinocytosis (Figure 3b). Note that the obtained mean values $\gamma = (2.20 \pm 1.45) \times 10^5$ J/m^4, and $\kappa = (2.28 \pm 0.51) \times 10^{-19}$ J for the healthy adult RBCs (i.e., no exposure to endotoxin lipid A) were comparable to the previously reported values obtained by fluctuation analyses.[37,38] In contrast, LPSs exhibited an increase in spring constant γ and a decrease in bending stiffness κ, accompanied by larger correlation coefficients. It should be noted that this tendency is much more pronounced for LPS Ra: Relative changes in the mean γ and κ were $\Delta\gamma = +159.2\%$ with the correlation coefficient of the ensemble *C.C.* = 0.526 and $\Delta\kappa = -47.6\%$ with *C.C.* = 0.673, respectively. Our finding implies that adult RBCs exposed to LPSs becomes softer against the bending deformation, meanwhile inflexible in the sense of shear. The increase in cytoskeleton-membrane coupling and thus the shear modulus suggested here qualitatively agrees with the decrease in deformability of RBCs treated with a LPS mutant with intact outer core region (LPS Rd from *Escherichia coli*) measured with a shear stress diffractometer.[39] This suggests that adult RBCs mechanically respond in a different manner against bending and shear stresses. It is notable that changes in the surface tension σ exhibited no systematic tendency in the presence and absence of endotoxins under the present conditions (see Figures S4 and S5 in the Supporting Information). Therefore, we focused on the impacts of LPS Ra on spring constant γ and bending stiffness κ in the following discussion.

Parts a and b of Figure 5 show the individual (gray lines) and the mean (black thick lines) values of γ and κ of neonatal RBCs in the presence and absence of 100 μg/mL LPS Ra. Relative changes in γ and κ exhibited the same tendency as those observed for adult RBCs. However, as shown in Figure 5c, relative changes in γ and κ of neonatal RBCs were more pronounced compared to those of adult RBCs. This finding seems reasonable from the fraction of RBCs undergoing echinocytosis, indicating that neonatal RBCs were more susceptible to endotoxins.

Furthermore, we investigated a possible curative effect of antiseptic peptide P19 after incubation with LPS Ra in a microfluidic diffusion chamber. Figure 6a shows the fractions of faceted RBCs and echinocytes before and after perfusion of 1 mg/mL P19 peptide accompanied by 100 μg/mL LPS Ra for adult and neonatal RBCs. The obtained results suggest P19 does not have neither toxicity to the discocyte shape nor curative effects on echinocytosis. However, the calculated mechanical parameters clearly indicate the curative effect of P19. Figure 6b and 6c show the relative changes in spring constant γ and bending stiffness κ caused by the perfusion of endotoxins. After perfusion of 1 mg/mL P19, both the relative changes in spring constant and bending stiffness slightly decreased: For adult RBCs $\Delta\kappa$ decreased from -47.6% (*C.C.* = 0.673) to -39.2% (*C.C.* = 0.529), and the corresponding values of neonatal RBCs were from -60.5% (*C.C.* = 0.619) to -61.6% (*C.C.* = 0.665). On the other hand, $\Delta\gamma$ for adult RBCs decreased from $+159.2\%$ (*C.C.* = 0.526) to $+131.5\%$ (*C.C.* = 0.506), and from $+268.2\%$ (*C.C.* = 0.599) to $+179.61\%$ (*C.C.* = 0.278) for neonatal RBCs.

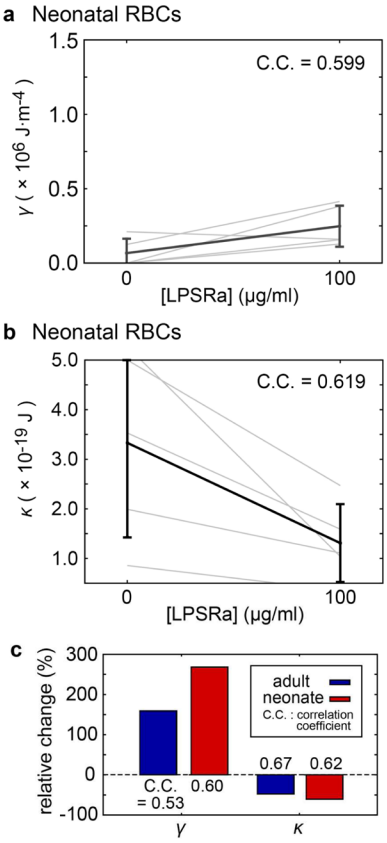

Figure 5. Changes in (a) spring constant γ and (b) bending stiffness κ of neonatal red blood cells caused by the additions of 100 μg/mL LPS Ra. The correlation coefficients *C.C.* are shown in the upper right of the graph. (c) Relative changes in the spring constant and bending stiffness caused by 100 μg/mL LPS Ra, suggesting that the impact of endotoxins (LPS) to the mechanics of discocytes are similar but more pronounced for neonatal red blood cells (red) compared to the adult red blood cells (blue).

4. DISCUSSION

Shape fluctuation and mechanics of cells have been of great interest within the framework of active soft matter physics. Betz et al. measured the power spectral density as a function of frequency in the presence and absence of ATP.[29] They reported that the equilibrium description breaks down at a characteristic frequency, and estimated the changes in "effective temperature". With aid of beads biochemically attached to cell surfaces, nonlinear frequency-response of RBCs can be monitored by fluctuation analysis.[40] In fact, such nonlinear response functions have been reported in various biological systems, such as isolated actomyosin complexes[41] and cytoplasm in living cells.[42] In this study, we analyzed the ATP-dependent coupling between cytoskeletons and cell membranes via spatial fluctuation spectra.[18,28,29,43]

4.1. Physical Mechanism of Echinocytosis. As presented in Figure 3, we found that both adult and neonatal RBCs undergo a morphological transition from normal discocyte to echinocyte when they are in contact with endotoxin (LPSs). Lim et al. explained this morphological transition in terms of the shape-free-energy functional that includes the bending energy of cell membranes, as well as the cytoskeletal elastic energy for stretching and shear.[44] It has been demonstrated that the morphological transition to echinocyte could be reproduced by increasing the area difference between inner and outer

DOI: 10.1021/acs.jpcb.5b01544
J. Phys. Chem. B 2015, 119, 7837−7845

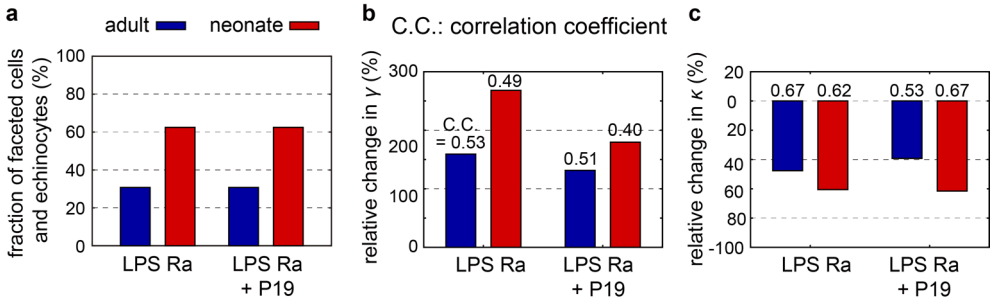

Figure 6. Impacts of antiseptic peptide P19 on the elastic properties of adult (blue) and neonatal (red) red blood cells, which were pretreated with 100 μg/mL LPS Ra. (a) Fractions of the faceted cells or echinocytes, relative changes in (b) spring constant γ and (c) bending stiffness κ caused by the addition of P19 (1 mg/mL). The correlation coefficients are shown above the corresponding bars.

leaflets. In our experiments, LPS molecules with six hydrocarbon chains, which are similar or shorter in lengths (C12 and C14) than those of the cell membrane lipids,[45] are incorporated into the cell membranes via perfusion from the bulk solution but not from inside, leading to an increase in the area of the outer leaflet.[46,47] Since the inner leaflet remains almost intact due to a negligibly little probability for flip-flop in our experimental time window, the difference in surface areas would serve as the driving force of the morphological transition. In fact, there have been several reports on the morphological transition of RBCs accompanied by the abnormality of lipid compositions caused by diseases like sickle cell anemia.[48] Therefore, the decrease in the bending stiffness we observed could be attributed to the lateral expansion of the outer leaflet caused by the incorporation of LPS molecules from the outside.

Previously, Warren et al. reported that the interaction of endotoxin and transmembrane band-3 as well as the incorporation of endotoxin molecules into the outer leaflet of RBC membranes could cause echinocytosis.[49] A more recent study demonstrated an elevated level of band-3 phosphorylation in septic mice, suggesting that the exposure to endotoxin increases the level of ATP consumption.[50] Therefore, it is plausible that the endotoxin-induced echinocytosis is a consequence of two effects: (i) the decrease in the bending stiffness κ by asymmetric incorporation of endotoxins into the outer leaflet, and (ii) the increase in spectrin-membrane coupling γ caused by the binding of endotoxin to band-3. The latter scenario needs to be verified by more precise determination of ATP level during the exposure to endotoxin.

4.2. Mechanics of Adult and Neonatal RBCs. The quantitative fluctuation analysis enables one to calculate the principal parameters describing the mechanics of not only adult (Figure 4) but also neonatal RBCs (Figure 5), although one cannot completely exclude a possibility that the changes in the parameters of echinocyte RBCs can be larger than those analyzed here for discocyte RBCs. Taking the theoretical model including bending stiffness κ, surface tension σ, and spring constant between membranes and cytoskeletons γ (eq 2),[24] we analyzed the experimentally measured mean square amplitude of closed cell membranes by eliminating the smaller wave numbers $\langle r \rangle q < 3$. First, we found that the bending stiffness and surface tension of neonatal RBCs are comparable to those of adult RBCs. On the other hand, the spring constant γ of neonatal RBCs is by 3−5 times smaller than that of adult RBCs. The shear elasticity of RBCs is dominated by that of the spectrin meshwork coupled to the membranes.[16,29] Since the spring constant γ is directly correlated to the shear modulus of RBCs, $\mu = A\gamma$,[24] where $A \sim 100\ \mu m^2$ is the surface area of a RBC, this finding suggests that the shear modulus of neonatal RBCs is smaller than that of adult RBCs.

On the basis of the fitting in the previous study, Yoon et al. reported that the impact of spring constant γ is negligibly smaller compared to bending stiffness κ and surface tension σ. This fact and eq 2 set an upper limit of spring constant γ for untreated adult RBCs to be $\gamma < 5 \times 10^5$ J/m^4, corresponding to the upper limit of shear modulus $\mu < 3 \times 10^{-5}$ N/m.[24] Actually, the mean values of γ for untreated adult RBCs that we calculated from the experimental results lies in the order of 10^5 J/m^4, which coincides with the shear modulus of $\mu \sim A\gamma \sim 10^{-5}$ N/m. This value is in good agreement with those measured by flicker spectroscopy[37] and by other techniques such as micropipet aspiration.[50,51] Therefore, we concluded that γ should not be neglected in the fluctuation analysis.

The experimentally obtained mean value for untreated neonatal RBCs, $\gamma \sim 5 \times 10^4$ J/m^4, is distinctly smaller than that of adult RBCs.[52] Previously, Linderkamp et al. demonstrated that neonatal RBCs are more deformable than adult RBCs with a smaller shear modulus.[5,53] Here, an increase in deformability coincides with a decrease in shear modulus, since the deformability was defined from the aspect ratio under shear flow. Although the deformability cannot be translated numerically to mechanical parameters, we found that the calculated shear modulus of neonatal RBCs, $\mu \sim 10^{-6}$ N/m, was actually 3−5 times smaller than that of adult RBCs. Thus, our quantitative experimental finding seems consistent with the cell deformation under micropipet aspiration. The mechanism of this softness of neonatal RBCs against shear deformation is still an open question. As one factor that could significantly influence the cell mechanics is the cytoskeletal remodeling powered by ATP hydrolysis, the large deformability of neonatal RBCs suggests that neonatal RBCs might contain higher amount of ATP. Previously, Kodama reported that the mean ATP concentration in neonatal blood is slightly lower than that in adult blood up to 4 h after the birth and increases to the comparable level to the adult after 1 d.[54] This suggests that the softness of neonatal RBCs cannot be explained by the ATP concentration difference. Therefore, our experimental finding suggests that ATP concentration is not the dominant factor that causes the difference in stiffness between neonatal and adult RBCs.

4.3. Impact of Molecular Chemistry. If one focuses on the impact of molecular structures of different LPSs on cell mechanics, the changes in the mechanical parameters, i.e., the decrease in κ and the increase in γ, were monotonically magnified according to the elongation of saccharide chain length (Figure 4). Our finding, the decrease in κ by the

DOI: 10.1021/acs.jpcb.5b01544
J. Phys. Chem. B 2015, 119, 7837−7845

exposure to LPSs, seems contradictory to our previous off-specular neutron scattering study on the LPS multilayers, where we found that the elongation of saccharide head groups of LPSs results in the increase in bending stiffness κ.[55] However, this apparent discrepancy can actually be explained if one takes the symmetry of membranes into account. Pure LPS membranes deposited on solid substrates for neutron scattering are symmetric, and thus the thickening of membranes due to the elongation of saccharide chain length results in an increase in the bending stiffness. On the other hand, LPS molecules are asymmetrically incorporated into the outer leaflet of RBC membranes. The asymmetric incorporation of "bulky" LPS molecules leads to a disordering of membrane lipids, which is supposed to cause a decrease in the bending stiffness. Indeed, the micropipet experiments by Evans and Rawicz demonstrated that the decrease in bending stiffness is caused by the decrease in lateral packing of lipids.[56]

If one compares the impact of LPS Ra on the RBC mechanics (Figure 5c), neonatal RBCs were found to be slightly more susceptible than adult RBCs, which can be characterized by a larger change in the spring constant γ. This finding suggests that LPSs would interact more strongly to neonatal RBCs and interfere with the coupling between spectrin cytoskeleton and cell membranes.

4.4. Impact of P19. We extend our approach by investigating the function of the peptide-based antisepsis drug P19. As presented in Figure 6, it was found that the coincubation of P19 with LPS Ra slightly reduced the impact of LPS Ra on RBC mechanics. Recently Abuillan et al. reported that P19 interacts much more significantly with LPS Ra compared to the naturally occurring cationic antibacterial peptide (herring protamine).[34] The stoichiometry of the reaction between P19 and LPS Ra determined by grazing incident X-ray fluorescence (about 1:3) was in excellent agreement with that obtained by isothermal titration calorimetry.[27,57,58] The previous studies reported that antiseptic peptide P19 has a strong binding capability to endotoxins, resulting in the formation of multilamellar P19-LPS complexes in bulk.[27] Therefore, the added P19 in bulk could result in a slight but distinct protection function against endotoxin insertion into RBC membranes by decreasing the equilibrium concentration of endotoxin molecules in the membranes. Moreover, the shape analysis (Figure 6a) and the correlation coefficient analysis of relative changes (Figure 6, parts b and c) suggest that the protection functions of P19 were slightly more significant for neonatal RBCs than for adult RBCs. However, it should be noted that the mechanical parameters of RBCs treated with LPS Ra and P19 were clearly different from those of untreated RBCs. Thus, we conclude that the LPS-P19 interaction is not strong enough to keep RBCs completely intact.

5. CONCLUSIONS

We presented a quantitative modeling of sepsis symptoms by calculating the mechanical properties of human RBCs from its shape fluctuation in the absence and presence of endotoxins (lipid A, LPS Re, LPS Ra) by the combination of noninvasive flicker spectroscopy and a microfluidic diffusion chamber. As sepsis is a life-threatening disease for neonates, we monitored for the first time the mechanical response of neonatal RBCs, in systematical comparison with adult RBCs. First, it was found that adult RBCs undergo a morphological transition from discocytes to echinocytes in the presence of endotoxins. In the next step, we calculated the mechanical parameters (bending stiffness κ, surface tension σ, and spring constant representing membrane-cytoskeleton coupling γ) of RBCs and found that exposure of RBCs with endotoxins leads to an increase in γ and a decrease in κ. Interestingly, the mechanical impact caused by endotoxins monotonically increased with the elongation of saccharide head groups. Neonatal RBCs were more susceptible to these effects of the endotoxins than adult RBCs. We also confirmed that the antiseptic peptide P19 can slightly suppress the effects of the endotoxin. The combination of flicker spectroscopy and a microfluidic device used here can noninvasively extract the elastic properties and their temporal variation by updating the surrounding condition, which allows for the physical diagnosis of suspended cells in contact with drugs and toxins based on mechanics.

■ ASSOCIATED CONTENT

Supporting Information

Perfusion test with fluorescent molecules, explanation of the fitting, and results of surface tension and spring constant. The Supporting Information is available free of charge on the ACS Publications website at DOI: 10.1021/acs.jpcb.5b01544.

■ AUTHOR INFORMATION

Corresponding Author

*(M.T.) E-mail: tanaka@uni-heidelberg.de.

Author Contributions

H.I., N.K., M.I., K.B., J.M.B.P., and M.T. designed the research; H.I., N.K., B.E.R., E.W., C.N., and T.G. performed the research; H.I. contributed analytic tools and analyzed data; all authors wrote the paper.

Notes

The authors declare no competing financial interest.

■ ACKNOWLEDGMENTS

H.I. is thankful to T. Ohmura, E. Wilhelm, and C. Neumann for their supports in microfluidic experiments, and T. Kenmotsu and M. Kaneko for helpful comments. We thank members in the Frühkindliche individuelle Pflegestation (FIPS) for the collection and preparation of blood samples. This work was supported by grants from EU FP7 "SoftActive", the Japan Society for the Promotion of Science (JSPS) Core-to-Core Program "non-equilibrium dynamics of soft matter and information," JSPS (26247070), and SPIRITS Program of Kyoto University. H.I. was supported by Grants-in-Aid for JSPS research Fellowship for Young Scientists (13J01297). M.T. and M.I. thank the Ministry of Education, Culture, Sports, Science, and Technology of Japan for supports "Fluctuation & Structure" (Nos. 26103521 and 25103012, respectively).

■ REFERENCES

(1) Lüderitz, O.; Freudenberg, M. A.; Galanos, C.; Lehmann, V.; Rietschel, E. T.; Shaw, D. H.; Felix, B.; Arnost, K. *Current Topics in Membranes and Transport*; Academic Press: New York, 1982.

(2) Raetz, C. R. H.; Ulevitch, R. J.; Wright, S. D.; Sibley, C. H.; Ding, A.; Nathan, C. F. Gram-Negative Endotoxin: an Extraordinary Lipid with Profound Effects on Eukaryotic Signal Transduction. *FASEB J.* **1991**, *5*, 2652−2660.

(3) Pöschl, J. M. B.; Linderkamp, O. Effect of Lipid A on the Deformability, Membrane Rigidity and Geometry of Human Adult Red Blood Cells. *Eur. J. Clin. Invest.* **1992**, *22*, 625−629.

(4) Pöschl, J. M. B.; Leray, C.; Ruef, P.; Cazenave, J. P.; Linderkamp, O. Endotoxin Binding to Erythrocyte Membrane and Erythrocyte

DOI: 10.1021/acs.jpcb.5b01544
J. Phys. Chem. B 2015, 119, 7837−7845

Deformability in Human Sepsis and *In Vitro*. *Crit. Care Med.* **2003**, *31*, 924−928.
(5) Linderkamp, O.; Pöschl, J.; Ruef, P. Blood Cell Deformation in Neonate Who Have Sepsis. *Neoreviews.* **2006**, *7*, 517−523.
(6) Pöschl, J. M.; Ruef, P.; Schnauffer, M.; Pohl, S.; Sonntag, H. G.; Linderkamp, O. Group B Streptococcus Impairs Erythrocyte Deformability in Neonates More Than in Adults. *Arch. Dis. Child.* **1996**, *74*, F187−F190.
(7) Suresh, S.; Spatz, J.; Mills, J. P.; Micoulet, A.; Dao, M.; Lim, C. T.; Beil, M.; Seufferlein, T. Connections Between Single-Cell Biomechanics and Human Disease State: Gastrointestinal Cancer and Malaria. *Acta Biomater.* **2005**, *1*, 15−30.
(8) Sleep, J.; Wilson, D.; Simmons, R.; Gratzer, W. Elasticity of the Red Cell Membrane and Its Relation to Hemolytic Disorders: An Optical Tweezers Study. *Biophys. J.* **1999**, *77*, 3085−3095.
(9) Guck, J.; Schinkinger, S.; Lincoln, B.; Wottawah, F.; Ebert, S.; Romeyke, M.; Lenz, D.; Erickson, H. M.; Ananthakrishnan, R.; Mitchell, D.; et al. Optical Deformability As an Inherent Cell Marker for Testing Malignant Transformation and Metastatic Competence. *Biophys. J.* **2005**, *88*, 3689−3698.
(10) Guck, J.; Ananthakrishnan, R.; Mahmood, H.; Moon, T. J.; Cunningham, C. C.; Käs, J. The Optical Stretcher: A Novel Laser Tool to Micromanipulate Cells. *Biophys. J.* **2001**, *81*, 767−784.
(11) Guck, J.; Ananthakrishnan, R.; Moon, T. J.; Cunningham, C. C.; Käs, J. Optical Deformability of Soft Biological Dielectrics. *Phys. Rev. Lett.* **2000**, *84*, 5451−5454.
(12) Peterson, M. A. Linear Response of the Human Erythrocyte to Mechanical Stress. *Phys. Rev. A* **1992**, *45*, 4116−4131.
(13) Gov, N.; Zilman, A. G.; Safran, S. Cytoskeleton Confinement and Tension of Red Blood Cell Membranes. *Phys. Rev. Lett.* **2003**, *90*, 228101.
(14) Brochard, F.; Lennon, J. F. Frequency Spectrum of the Flicker Phenomenon in Erythrocytes. *J. Phys. (Fr.).* **1975**, *36*, 1035−1047.
(15) Helfrich, W.; Servuss, R. M. Undulations, Steric Interaction and Cohesion of Fluid Membranes. *Nuovo Cimento D* **1984**, *3*, 137−151.
(16) Peterson, M. A.; Strey, H.; Sackmann, E. Theoretical and Phase Contrast Microscopic Eigenmode Analysis of Erythrocyte Flicker: Amplitudes. *J. Phys. II France.* **1992**, *2*, 1273−1285.
(17) Strey, H.; Peterson, M.; Sackmann, E. Mesurement of Erythrocyte Membrane Elasticity by Flicker Eigenmode Decomposition. *Biophys. J.* **1995**, *69*, 478−488.
(18) Gov, N. S.; Safran, S. A. Red Blood Cell Membrane Fluctuations and Shape Controlled by ATP-Induced Cytoskeletal Defects. *Biophys. J.* **2005**, *88*, 1859−1874.
(19) Discher, D. E.; Mohandas, N.; Evans, E. A. Molecular Maps of Red Blood Cell Deformation: Hidden Elasticity and In Situ Connectivity. *Science.* **1994**, *266*, 1032−1035.
(20) Heinrich, V.; Ritchie, K.; Mohandas, N.; Evans, E. Elastic Thickness Compressibility of the Red Cell Membrane. *Biophys. J.* **2001**, *81*, 1452−1463.
(21) Engelhardt, H.; Gaub, H.; Sackmann, E. Viscoelastic Properties of Erythrocyte Membranes in High-Frequency Electric Fields. *Nature.* **1984**, *307*, 378−380.
(22) Engelhardt, H.; Sackmann, E. On the Measurement of Shear Elastic Moduli and Viscosities of Erythrocyte Plasma Membranes by Transient Deformation in High Frequency Electric Fields. *Biophys. J.* **1985**, *54*, 495−508.
(23) Peterson, M. A. Shape Dynamics of Nearly Spherical Membrane Bounded Fluid Cells. *Mol. Cryst. Liq. Cryst.* **1985**, *127*, 257−272.
(24) Yoon, Y.-Z.; Hong, H.; Brown, A.; Kim, D. C.; Kang, D. J.; Lew, V. L.; Cicuta, P. Flickering Analysis of Erythrocyte Mechanical Properties: Dependence on Oxygenation Level, Cell Shape, and Hydration Level. *Biophys. J.* **2009**, *97*, 1606−1615.
(25) Pécréaux, J.; Döbereiner, H.-G.; Prost, J.; Joanny, J.-F.; Bassereau, P. Refined Contour Analysis of Giant Unilamellar Vesicles. *Eur. Phys. J. E* **2004**, *13*, 277−290.
(26) Vrhovec, S.; Mally, M.; Kavcic, B.; Derganc, J. A Microfluidic Diffusion Chamber for Reversible Environmental Changes Around Flaccid Lipid Vesicles. *Lab Chip.* **2011**, *11*, 4200−4206.
(27) Brandenburg, K.; Andrä, J.; Garidel, P.; Gutsmann, T. Peptide-Based Treatment of Sepsis. *Appl. Microbiol. Biotechnol.* **2011**, *90*, 799−808.
(28) Tuvia, S.; Almagor, A.; Bitler, A.; Levin, S.; Korenstein, R.; Yedgar, S. Cell Membrane Fluctuations Are Regulated by Medium Macroviscosity: Evidence for a Metabolic Driving Force. *Proc. Natl. Acad. Sci. U.S.A.* **1997**, *94*, 5045−5049.
(29) Betz, T.; Lenz, M.; Joanny, J.-F.; Cykes, C. ATP-Dependent Mechanics of Red Blood Cells. *Proc. Natl. Acad. Sci. U.S.A.* **2009**, *106*, 15320−15325.
(30) Galanos, C.; Ludëritz, O.; Westphal, O. A New Method for the Extraction of R Lipopolysaccharides. *Eur. J. Biochem.* **1969**, *9*, 245−249.
(31) Brandenburg, K.; Seydel, U. Physical Aspects of Structure and Function of Membranes Made from Lipopolysaccharides and Free Lipid A. *Biochim. Biophys. Acta* **1984**, *775*, 225−238.
(32) Rietschel, E. T.; Wollenweber, H. W.; Brade, H.; Zähringer, U.; Lindner, B.; Seydel, U.; Bradaczek, H.; Barnickel, G.; Labinschinski, H.; Giesbrecht, P. *Handbook of Endotoxin*; Rietschel, E. T., Ed.; Elsevier: Amsterdam, 1984.
(33) Schuerholz, T.; Brandenburg, K.; Marx, G. Antimicrobial Peptides and Their Potential Application in Inflammation and Sepsis. *Crit. Care* **2012**, *16*, 207.
(34) Abuillan, W.; Schneck, E.; Körner, A.; Brandenburg, K.; Gutsmann, T.; Gill, T.; Vorobiev, A.; Konovalov, O.; Tanaka, M. Physical Interactions of Fish Protamine and Antisepsis Peptide Drugs with Bacterial Membranes Revealed by Combination of Specular X-Ray Reflectivity and Grazing-Incidence X-Ray Fluorescence. *Phys. Rev. E* **2013**, *88*, 012705.
(35) Waldbaur, A.; Carneiro, B.; Hettich, P.; Wilhelm, E.; Rapp, B. Computer-Aided Microfluidics (CAMF): From Digital 3D-CAD Models to Physical Structures Within a Day. *Microfluid. Nanofluid.* **2013**, *15*, 625−635.
(36) Thévenaz, P.; Blu, T.; Unser, M. Interpolation Revisited. *IEEE Trans. Med. Imaging* **2000**, *19*, 739−758.
(37) Hale, J. P.; Winlove, P.; Petrov, P. G. Effect of Hydroperoxides on Red Blood Cell Membrane Mechanical Properties. *Biophys. J.* **2011**, *101*, 1921−1929.
(38) Mesquita, L. G.; Agero, U.; Mesquita, O. N. Defocusing Microscopy: An Approach for Red Blood Cell Optics. *Appl. Phys. Lett.* **2006**, *88*, 133901.
(39) Pöschl, J. M. B.; Ruef, P.; Schnauffer, M.; Linderkamp, O. The Effect of Different Escherichia Coli Endotoxins on Red Blood Cell Deformability. *Clin. Hemorheol.* **1995**, *15*, 749−753.
(40) Yoon, Y. Z.; Kotar, J.; Brown, A. T.; Cicuta, P. Red Blood Cell Dynamics: From Spontaneous Fluctuations to Non-linear Response. *Soft Matter* **2011**, *7*, 2042−2051.
(41) Mackintosh, F. C.; Levine, A. J. Nonequilibrium Mechanics and Dynamics of Motor-Activated Gels. *Phys. Rev. Lett.* **2008**, *100*, 018104.
(42) Guo, M.; Ehrlicher, A. J.; Jensen, M. H.; Renz, M.; Moore, J. R.; Goldman, R. D.; Lippincott-Schwartz, J.; Mackintosh, F. C.; Weitz, D. A. Probing the Stochastic, Motor-Driven Properties of the Cytoplasm Using Force Spectrum Microscopy. *Cell* **2014**, *158*, 822−832.
(43) Park, Y.; Best, C. A.; Auth, T.; Gov, N. S.; Safran, S. A.; Popescu, G.; Suresh, S.; Feld, M. S. Metabolic Remodeling of the Human Red Blood Cell Membrane. *Proc. Natl. Acad. Sci. U.S.A.* **2010**, *107*, 1289−1294.
(44) Lim, H. W. G.; Wortis, M.; Mukhopadhyay, R. Stomatocyte-Discocyte-Echinocyte Sequence of the Human Red Blood Cell: Evidence for the Bilayer-Couple Hypothesis from Membrane Mechanics. *Proc. Natl. Acad. Sci. U.S.A.* **2002**, *99*, 16766−16769.
(45) van Deenen, L. L. M.; Op den Kamp, J. A. F.; Roelofsen, B.; Wirtz, K. W. A. On Membrane Phospholipids and Protein-Lipid Association. *Pure Appl. Chem.* **1982**, *54*, 2443−2454.
(46) Sheetz, M. P.; Singer, S. J. Biological Membranes as Bilayer Couples. A Molecular Mechanism of Drug-Erythrocyte Interactions. *Proc. Natl. Acad. Sci. U.S.A.* **1974**, *71*, 4457−4461.
(47) Fujii, T.; Sato, T.; Tamura, A.; Wakatsuki, M.; Kanaho, Y. Shape Changes of Human Erythrocytes Induced by Various Amphipathic

DOI: 10.1021/acs.jpcb.5b01544
J. Phys. Chem. B 2015, 119, 7837−7845

Drugs Acting on the Membrane of the Intact Cells. *Biochem. Phrmacol.* **1979**, *28*, 613−620.
(48) Lubin, B.; Chiu, D.; Bastacky, J.; Roelofsen, B.; van Deenen, L. L. M. Abnormalities in Membrane Phospholipid Organization in Sickled Erythrocytes. *J. Clin. Invest.* **1981**, *67*, 1643−1649.
(49) Warren, J. R.; Harris, A. S.; Wallas, C. H. Transformation of Human Erythrocyte Shape by Endotoxic Lipopolysaccharide. *Infect. Immun.* **1983**, *39*, 431−434.
(50) Condon, M. R.; Feketova, E.; Machiedo, G. W.; Deitch, E. A.; Spolarics, Z. Augmented Erythrocyte Band-3 Phosphorylation in Septic Mice. *Biochim. Biophys. Acta* **2007**, *1772*, 580−586.
(51) Waugh, R.; Evans, E. A. Thermoelasticity of Red Blood Cell Membrane. *Biophys. J.* **1979**, *26*, 115−131.
(52) Hochmuth, R. M. Solid and Liquid Behavior of Red Cell Membrane. *Annu. Rev. Biophys. Bioeng.* **1982**, *11*, 43−55.
(53) Linderkamp, O.; Nash, G. B.; Wu, P. Y. K.; Meiselman, H. J. Deformability and Intrinsic Material Properties of Neonatal Red Blood Cells. *Blood.* **1986**, *67*, 1244−1250.
(54) Kodama, C. Clinical Studies on ATP Concentration in the Blood of Mother and Newborn Infant, Especially on the Relationship with the Infant Jaundice. *Adv. Obstet. Gynecol.* **1971**, *23*, 196−215.
(55) Schneck, E.; Oliveira, R. G.; Rehfeldt, F.; Demé, B.; Brandenburg, K.; Seydel, U.; Tanaka, M. Mechanical Properties of Interacting Lipopolysaccharide Membranes from Bacteria Mutants Studied by Specular and Neutron Scattering. *Phys. Rev. E* **2009**, *80*, 041929.
(56) Evans, E.; Rawicz, W. Entropy-Driven Tension and Bending Elasticity in Condensed-Fluid Membranes. *Phys. Rev. Lett.* **1990**, *64*, 2094−2097.
(57) Gutsmann, T.; Razquin-Olazarán, I.; Kowalski, I.; Kaconis, Y.; Howe, J.; Bartels, R.; Hornef, M.; Schürholz, T.; Rössle, M.; Sanchez-Gómez, S.; et al. New Antiseptic Peptides To Protect against Endotoxin-Mediated Shock. *Antimicrob. Agents Chemother.* **2010**, *54*, 3817−3824.
(58) Kaconis, Y.; Kowalski, I.; Howe, J.; Brauser, A.; Richter, W.; Razquin-Olazaran, I.; Inigo-Pestana, M.; Garidel, P.; Rossle, M.; de Tejada, G. M.; et al. Biophysical Mechanisms of Endotoxin Neutralization by Cationic Amphiphilic Peptides. *Biophys. J.* **2011**, *100*, 2652−2661.

DOI: 10.1021/acs.jpcb.5b01544
J. Phys. Chem. B 2015, 119, 7837−7845